Theoretical demonstration of the hybrid focusing points of sonic crystal flat lenses and possible applications

Serkan Alagoz[a)†] and Baris Baykant Alagoz[b)]

[a)] Department of Physics, Inonu University, Center Campus, Malatya
[b)] Department of Electric-Electronics, Inonu University, Center Campus, Malatya

(Received 27 December 2012; revised manuscript received 12 February 2013)

We demonstrate the hybrid focusing points of sonic crystals for a multi-source array applied to flat sonic crystal lenses. The contributions of different point source couples form hybrid focusing points. Ray-trace analyses are conducted for acoustic flat lenses with multi-source configurations. The finite-difference time-domain (FDTD) simulation of flat lenses with multi-source configurations demonstrates the establishment of pure and hybrid focusing points in a pyramidal constellation. The number of focusing points in the pyramidal constellation depends on the number of point sources. We propose an acoustic device for fine-tuning the location of a far-field hybrid focusing point and discuss its benefits for acoustic energy focusing application.

Keywords: negative refraction, sonic crystal metamaterials, wave focusing, acoustic flat lens

PACS: 62.65.+k, 43.20.El, 43.35.Cg **DOI:** 10.1088/1674-1056/22/7/076201

1. Introduction

Metamaterials have been implemented by using artificial crystal structures for a wide range of wave spectra. Photonic crystals,[1–12] phononic crystals,[13–23] and sonic crystals[24–28] were developed for their technological potentials such as wave focusing,[24–31] wave isolation,[16–18,21] wave absorption,[10,22] and wave guiding.[2–4,32,33] The realization of flat lenses from crystal structures is one of the promising applications of metamaterials. Negative refraction and the wave focusing effects of negative refractive crystal slabs have been well studied in the last decade.[24–28] Those studies mainly addressed the focusing effect of single point source configurations. Reports indicated that flat lenses made of negative refractive crystals exhibited superior focusing properties, such as sub-wavelength focusing[31] and the ideal imaging effect.[24] The ideal imaging appears when the negative effective refraction index (ERI) of a crystal slab is equal to -1, in this case, the negative refractive flat lens provides a sharper image of a point source.[24,25,31]

The classical ray-trace analysis of negative refractive crystal slabs with a single point source considers a gathering of beam intersection points in a narrow region as the focusing points. One of them appears inside and the other appears outside of the crystal slabs. They have been analyzed by the ray-trace technique, and the results have been validated by finite-difference time-domain (FDTD) simulations and experimental measurements.[24,25,29–31]

This study extends the investigation to multiple monochromatic point sources applied to a flat lens made of a triangular lattice sonic crystal. Identical sources are arranged to line up in front of the sonic flat lens in the ray-trace analysis. This setup can produce an arrangement of focusing points in the pyramidal formation, as presented in Fig. 1. Two types of focusing points are observed in these pyramidal arrangements. The first type is produced solely by beams from each point source, referred to as pure focusing points in this study. Points i_1, i_2, and i_3 in Fig. 1 are pure focusing points. The second type of focusing points result from beams emitted from two separate point sources, hereafter referred to as hybrid focusing points. In Fig. 1, points $j_{1,2}$, $j_{2,3}$, $i_{1,2}$, $i_{2,3}$, and $i_{1,3}$ are hybrid focusing points.

The previous works extensively studied the pure focusing points for single-point source cases.[24–27] This paper specifically investigates multi-point source configurations that lead to the occurrences of hybrid focusing points. The shape of the focusing point constellation corresponds to two situations listed below. i) When there is no occurrence of the hybrid focusing point inside the crystal slab, as shown in Fig. 1(a), focusing points i_1, i_2, and i_3 are the pure focusing points, and the forward hybrid focusing points $i_{1,2}$, $i_{2,3}$, and $i_{1,3}$ appear next to the flat lens. ii) When hybrid focusing points exist inside the crystal slab, as shown in Fig. 1(b), backward hybrid focusing points $j_{1,2}$ and $j_{2,3}$ appear between the flat lens and the pure focusing points in addition to focusing points i_1, i_2, i_3, $i_{1,2}$, $i_{2,3}$, and $i_{1,3}$. The hybrid focusing points are caused by the interaction of wavefronts from different point sources, which behave as converging wavefronts.

†Corresponding author. E-mail: serkan.alagoz@inonu.edu.tr

© 2013 Chinese Physical Society and IOP Publishing Ltd

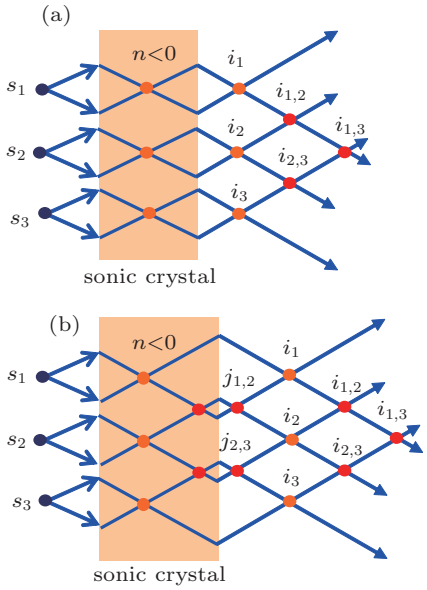


Fig. 1. (color online) Ray-trace drawings of possible focusing point pyramid compositions for point source combination (s_1, s_2, s_3). (a) When there are no hybrid focusing points inside the crystal (situation 1), the focusing point pyramid contains pure and forward hybrid focusing points. (b) When hybrid focusing exists inside the crystal, backward hybrid focusing points appear in the focusing point pyramid.

Two sonic crystal slabs are used in the FDTD simulation of the multi-source flat lens configurations. The first acoustic flat lens has a triangular lattice configuration with a lattice constant of 15 mm, a scatter radius of 5 mm, and a slab width of 110 mm. The multi-source array is 50 mm away from the crystal slab ($D_1 = 50$ mm). The distance between the point sources (e) is 52 mm. The second acoustic flat lens has a triangular lattice sonic crystal with a lattice constant of 25 mm, a scatter radius of 10 mm, and a slab width of 300 mm. The distance between the acoustic sources is 90 mm, and the distance between the source array and the crystal slab is 50 mm.

The paper is organized as follows. A ray trace analysis is developed for the hybrid focusing point in Section 2. Then, band structure analyses and FDTD simulations are demonstrated for test crystals. In Section 5, a possible application based on the control of the hybrid focusing points is presented for sonic crystal flat lenses.

2. Ray-trace analysis of multiple-point-source configurations

Figure 2(a) shows the ray-trace analysis of a crystal slab with a single source.[24–26] The intersection of beams indicates a wave focusing at the intersection point. In the case of a point source array placed near to a negative refractive sonic crystal, there appear several focusing points due to the intersections of the beams coming from different wave source couples (s_x, s_y), as shown in Fig. 2(b). To constitute a general notation, the forward hybrid focusing points are denoted as $i_{x,y}$, $x,y \in \{1,2,\ldots,m\}$. The forward hybrid focusing points are next to pure focusing points i_x. The backward hybrid focusing points reside between pure focusing points i_x and the crystal slab, and are denoted as $j_{x,y}$ ($x,y \in \{1,2,\ldots,m\}$). Here, m denotes the number of point sources lined up in front of the sonic flat lens. In a pyramidal arrangement of focusing points formed by m point sources, the total number of focusing points, N_m, can be written as

$$N_m = \begin{cases} \frac{1}{2}(m^2+m), & \text{for situation 1,} \\ \frac{1}{2}(m^2+3m-2), & \text{for situation 2.} \end{cases} \quad (1)$$

The total number of hybrid focusing points, H_m, can be written as

$$H_m = \begin{cases} \frac{1}{2}(m^2-m), & \text{for situation 1,} \\ \frac{1}{2}(m^2+m-2), & \text{for situation 2.} \end{cases} \quad (2)$$

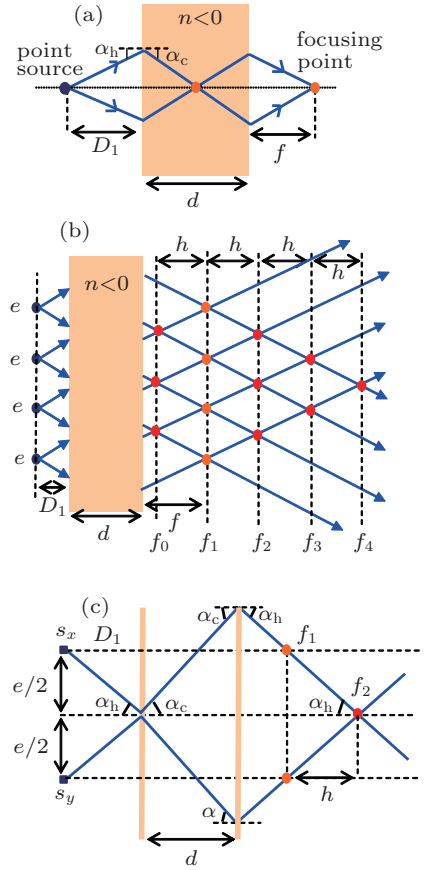


Fig. 2. (color online) (a) Focusing points of the negatively refractive crystal for a single wave source. (b) Focusing point arrangement of the negatively refractive crystal for multiple point sources, which are lined up at the interval of e. (c) A geometrical analysis on the ray-trace analysis of two point sources.

In the ray-trace analyses for a single point source, as illustrated in Fig. 2(a), the distance of a focusing point from the crystal was derived as $f = d/|n| - D_1$ in Refs. [24] and [25], where parameter $|n|$ represents the magnitude of negative ERI. We adopt this formula to estimate the distances of the hybrid focusing points from the crystal. The following assumptions are made to ensure that all focusing points reside at the corners of equally sized diamonds, as shown in Fig. 2(b).

(i) All point sources line up in front of a crystal, and they have an equal distance to the crystal interface (D_1) and an equal distance to each other (e).

(ii) The sonic crystal slab width d is large enough to allow the occurrence of pure focusing points.

(iii) Distances between the wave sources (e) are adjusted so that the focusing points are distinguishable from each other and the pyramidal constellation is apparent.

Under these assumptions, and considering the geometrical illustration in Fig. 2(b), we can derive the following sequence: $f_0 = f - h$, $f_1 = f$, $f_2 = f + h$, $f_3 = f + 2h$, and so on. Here, f_0 represents the distance of the backward hybrid focusing points to the crystal interface, f_1 represents the distance of the pure focusing points to the crystal interface, and f_p ($p \in [2, m]$) represents the distance of the forward hybrid focusing points to the crystal interface. The f_p for $p \in [0, m]$ can be expressed as

$$f_p = d/|n| - D_1 + (p-1)h. \tag{3}$$

By the geometrical analysis given for the effective beams coming from two sources (s_x, s_y) in Fig. 2(c), h can be expressed as $e/(2\tan\alpha_h)$. The parameter α_h denotes the angle of the effective incident beam to the normal of the flat lens interface. The effective incident beams are assumed to pass through a pure focusing point and at least one hybrid focusing point. The effective incident beam angel (α_h) and the magnitude of the ERI ($|n|$) for a sonic crystal flat lens design can be calculated by solving Eq. (3) for two focalization points.

3. Band structure analysis

This section presents the band structure characteristics of the test crystals used to discover the frequency band, where the sonic crystal slabs exhibit an ERI and behave as negative refractive flat lenses.

One of the promising properties of sonic crystal metamaterials is their negative ERI, appearing in the second frequency band of the sonic crystals. The band structure characteristics of triangular lattice sonic crystals in the second band present a convex form around high symmetry point Γ, which implies that the crystal slab exhibits a negative ERI within the second band.[1,3] Because wave vector $\boldsymbol{k}$ and group velocity vector $\boldsymbol{v}_g = \nabla_{\boldsymbol{k}} w(\boldsymbol{k})$ are opposite in direction, $\boldsymbol{k} \cdot \boldsymbol{v}_g < 0$.

The plane-wave expansion (PWE) method is commonly used to calculate the band structure characteristics of crystal structures.[3–6,17,18,24,25,31,34–36] The plane-wave method has been implemented in Matlab as in Ref. [36]. Figure 3 shows the band structure analyses of two test crystals. The convex form of the second band curves around Γ in Figs. 3(a) and 3(b) indicates a negative ERI. At the lower boundary of the second band, the test sonic crystal slabs work as a flat lens because they exhibit the negative ERI required for obtaining a far-field focusing effect.[28] The first test crystal can work as a flat lens at 16000 Hz, and the second test crystal can be utilized as a flat lens at 9300 Hz. The ERI at 16000 Hz in Fig. 3(a) and that at 9300 Hz in Fig. 3(b) are estimated to be -0.78 and -0.64, respectively. The FDTD simulation validates the focusing effects at these frequencies; the results will appear in the following section.

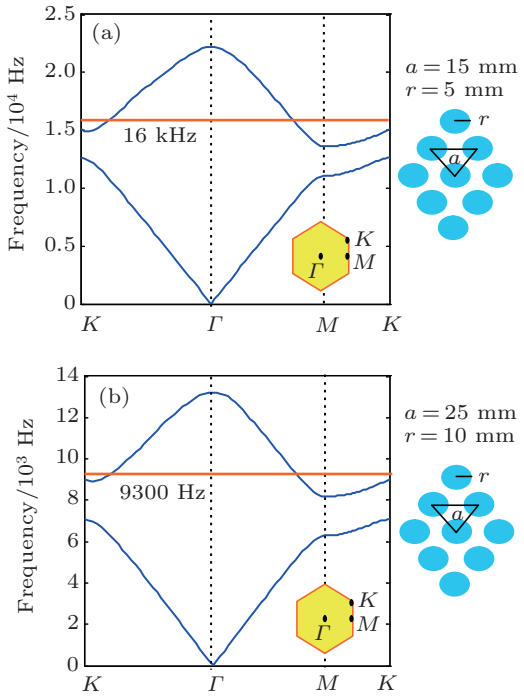


Fig. 3. (color online) Band structure analysis of triangular lattice sonic crystals used as flat lenses. A relevant focusing effect occurs (a) at 16000 Hz for the first flat lens and (b) at 9300 Hz for the second flat lens.

4. FDTD simulations of acoustic flat lens for multi-source configurations

The following wave equations are used in the FDTD-based simulation of acoustic wave propagation in a two-state medium:[36]

$$\frac{\partial \boldsymbol{v}}{\partial u} = -\rho \nabla p, \qquad \frac{\partial p}{\partial u} = -K \nabla \cdot \boldsymbol{v}, \tag{4}$$

where $\boldsymbol{v}$ denotes the normalized particle velocity, $\boldsymbol{v} = \rho_h c_0 \boldsymbol{V}$. The material parameters of the crystal structures are described by the normalized medium density, $\rho = \rho_h/\rho_s$, and the normalized bulk modulus, $K = K_s/K_h$. Here, ρ_h is the density of the host material, K_h is the bulk modulus of the host material, ρ_s and K_s are the corresponding parameters for the scattering material. Parameter u is the normalized time, $u = c_0 t$, where c_0 is the speed of sound in the host material, and t is the time.

FDTD simulation results, presented in Figs. 4 and 5, show normalized pressure-field (p) patterns and maximum normalized pressure-field intensity distributions in logarithmic scale ($\log_{10}(p^2_{max})$) for the cases of one, two, three, and four monochromatic point sources applied to the first test lens. The

point source arrays are composed of identical sources operating at 16000 Hz. A pure focusing point is obtained for a single point source configuration, as shown in Figs. 4(a) and 5(a). In the case of more than one point sources, forward hybrid focusing points, in addition to pure focusing points, are clearly observable, as shown in Figs. 4(b)–4(d) and 5(b)–5(d). The arrangement of focusing points in the simulation results confirms the pyramidal constellation in the ray-trace analyses.

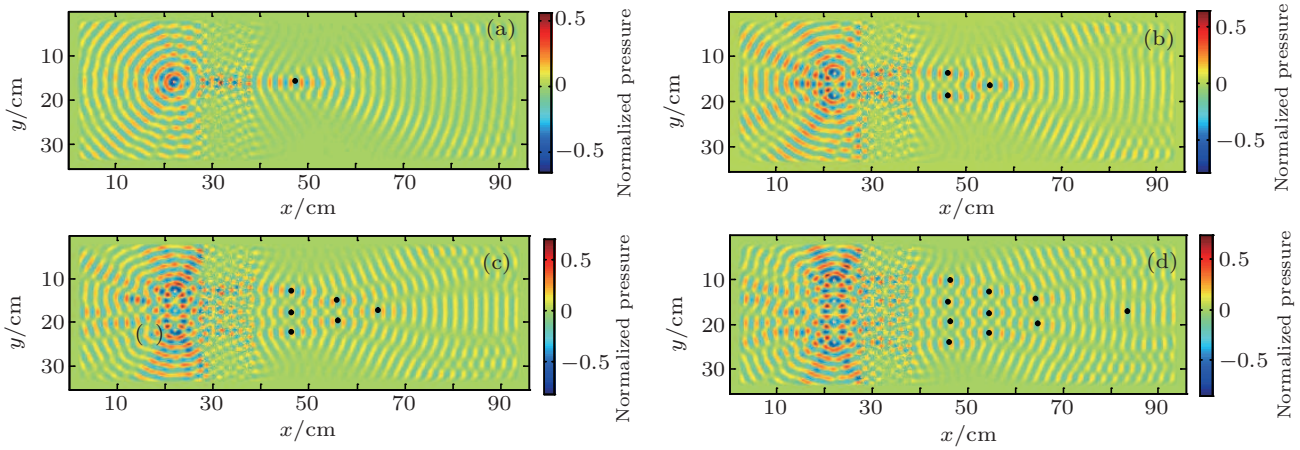


Fig. 4. (color online) Pressure wave propagation images from FDTD-based simulation results, showing the pyramidal arrangements of pure and forward hybrid focusings generated by the first test lens in the cases of (a) one, (b) two, (c) three, and (d) four monochromatic point sources.

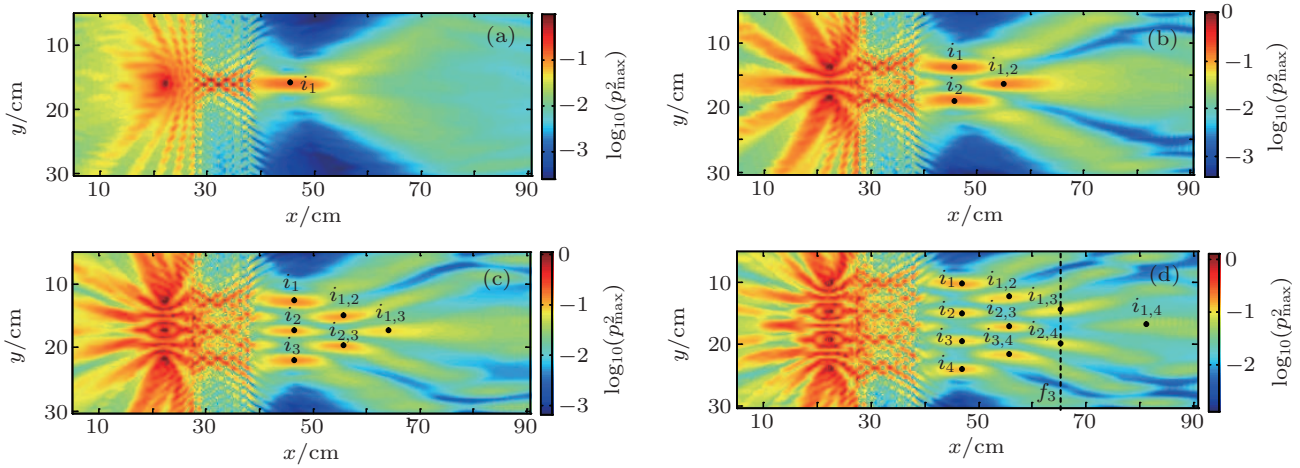


Fig. 5. (color online) Logarithmic scaled maximum-intensity maps ($\log_{10}(p^2_{\max})$) from FDTD-based simulation results, showing the pyramidal arrangements of pure and forward hybrid focusings generated by the first test lens in the cases of (a) one, (b) two, (c) three, and (d) four monochromatic point sources.

Figure 6 shows the backward hybrid focusing points generated by the second test lens. The point source array is composed of identical sources operating at 9300 Hz. A backward hybrid focusing is not generated via the first test lens in Fig. 5 because the width of the first flat lens is not large enough to contain a hybrid focusing point inside the crystal slab. The arrangement of the focusing points in the simulation results is consistent with the ray-trace analysis in Fig. 1(b).

The forward focusing points further than f_3 can be seriously distorted, since the sonic crystals cannot form apparent focalization points further than f_3. This effect is found in the ray-trace analyses as the spread of the distribution of the beam intersections of different angle beams over a wide area. This spreading indicates that the wave focalization region broadens and therefore reduces the peak intensity of the focusing point.

In the ray-trace analysis, the distribution of the beam intersection points in the focalization region can be used to asses the size and intensity of the hybrid focalization. When all beams converge to a narrow spot, the beam intersection points gather in the spot, resulting in a higher peak intensity in a narrow focalization region. The hybrid wave focalizations, which are far from the pure focusing points, are severely deteriorated due to the spreading of beam intersections over a wider region.

The ray-trace analysis is an efficient analytical tool for the evaluation of the wave focalization quality, however the Huygens principles well explain the wavefront mechanics resulting in the wave focalization. Figure 7 illustrates the relation between ray-trace and converging Huygens wavefronts. Fig-

ure 7(a) illustrates a converging wavefront (CW), a focalization region (FR), and a diverging wavefront (DW) according to the Huygens principles. Beams accompanying the wavefronts show us the possible wave focalization region. The wavefront fractions move along the directions of the arrows following the beams. Thus, gathering beam intersection points in a region in ray-trace indicate a possible wavefront convergence. Figure 7(b) shows the zoomed pressure-field patterns of pure (i_1, i_2) and hybrid ($i_{1,2}$) focusing points from the simulation in Fig. 4(b). The wavefront convergences and divergences are evident in the figure for the pure focusing points (CW_1, CW_2) and the hybrid focusing point (CW_{12}). The convex form of the diverging wavefronts from the neighbor pure focusing points leads to the build-up converging wavefronts (CW_{12}) of the hybrid focusing point ($i_{1,2}$) in the near field because of the coupling of phase coherent diverging wavefronts. This coupled near-field interaction between wave parts of pure focusing points causes these parts behaving as converging waves. The effect forms the hybrid focusing points. The figure reveals that the downside of diverging wavefront of i_1 and the upside of diverging wavefront of i_2 support the wavefront convergence CW_{12} forming hybrid focusing point $i_{1,2}$.

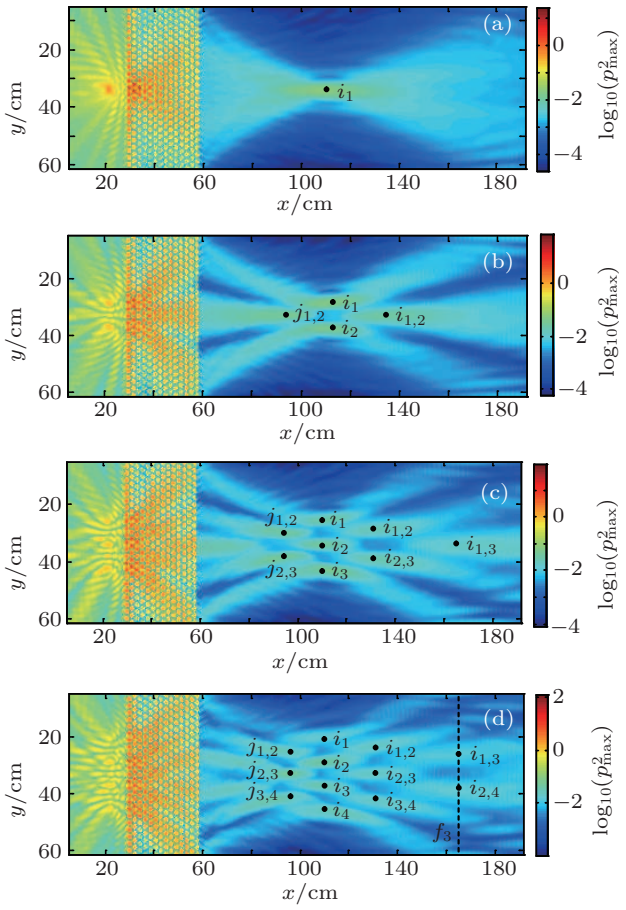


Fig. 6. (color online) Logarithmic scaled maximum-intensity maps ($\log_{10}(p^2_{\max})$) from FDTD-based simulation results, showing the backward hybrid focusing points $j_{1,2}$ and $j_{2,3}$ generated by the second test lens in the cases of (a) one, (b) two, (c) three, and (d) four monochromatic point sources.

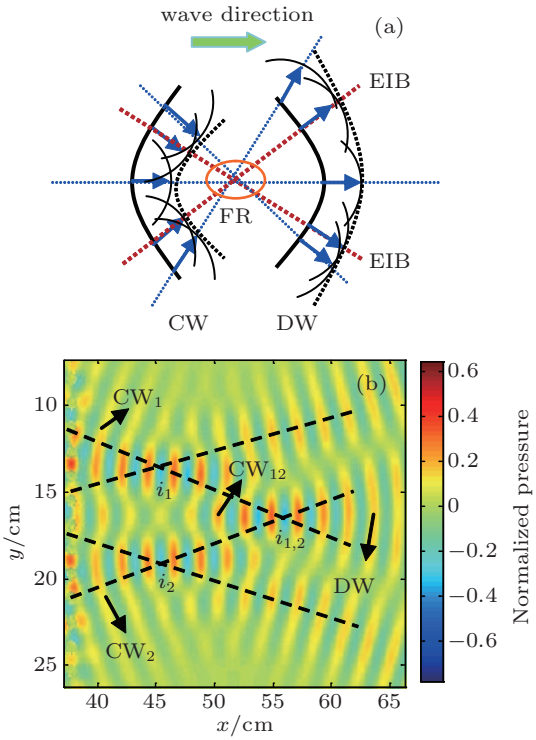


Fig. 7. (color online) (a) Wave focalization according to the Huygens principles, where EIB stands for the effective incident beam. (b) Pressure wave propagation image from FDTD-based simulation of the first flat lens, which shows the wave focalization according to the Huygens principles and the corresponding effective incident beams passing the sonic crystal.

5. Possible application: focal-point tunable double-source acoustic flat lenses

Steering of wave focalization location is useful for energy transmission applications.[37–41] We present a possible application of hybrid focusing points for the fine tuning of the far-field wave focalization region. The proposed acoustic device produces only the most distant forward hybrid focusing point in the pyramidal constellation and eliminates the rest of focusing points by wave blockading. Figure 8 shows a schematic diagram of the proposed acoustic device, which is made of a double-source flat lens with half-side wave blockages. This acoustic device can provide a more distant wave focalization compared to its single-source counterparts. Moreover, the location of the focalization region can be controlled by adjusting the distance between point sources (e). This allows us to steer the location of the focalization region without altering any structural parameters of the crystal slab or the acoustic wave frequency.

In order to allow only the peak hybrid focusing point and inhibit the rest of the focusing points in the pyramidal constellation, we apply wave blockages to the negative refractive flat lens, as shown in Fig. 8(a). These blockages eliminate the upper-side beams from source s_1 and the downside beams from source s_2, resulting in the removal of the pure focusing points i_1, i_2 and the backward hybrid focusing point $j_{1,2}$. On

the other hand, the cooperation of the downside beams from s_1 and the upper-side beams from s_2 generates only the most distant hybrid focusing point $i_{1,2}$.

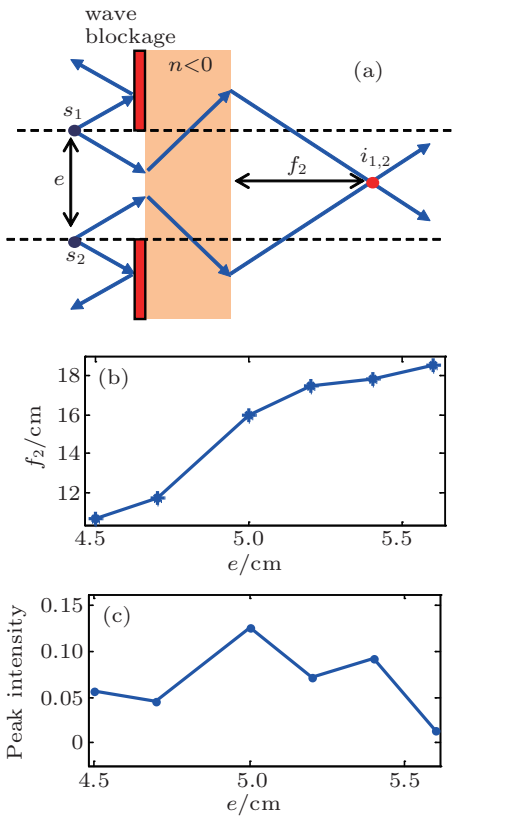


Fig. 8. (color online) (a) Schematic diagram of a double-source hybrid focusing point generator and its ray-trace analysis. (b) Distance of the hybrid focusing point $i_{1,2}$ (f_2) versus e from FDTD simulation. (c) Peak intensity of the hybrid focusing point $i_{1,2}$ versus e from FDTD simulation.

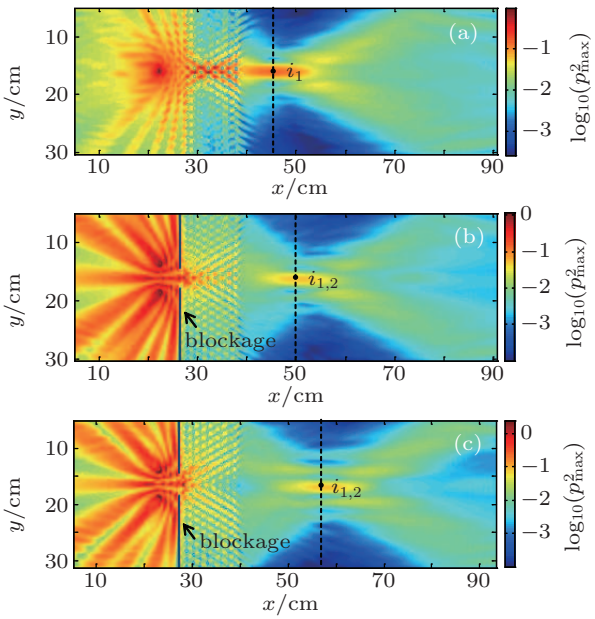


Fig. 9. (color online) (a) Logarithmic scaled maximum-intensity map ($\log_{10}(p^2_{\max})$) for a single point source generating a pure focusing point. Logarithmic scaled maximum-intensity maps for the double-source hybrid focusing point generator with (b) $e = 4.5$ cm, (c) $e = 5.4$ cm.

Figure 8(b) illustrates the dependence of the hybrid focusing point $i_{1,2}$ distance (f_2) on parameter e. The roughly 1 cm deviation in e results in a shift of the $i_{1,2}$ point in about 7 cm. Figure 8(c) shows the peak intensities for various values of e. Figures 9(a)–9(c) compare the far-field focusing point locations for the single point source configuration with those for the double-source configurations with wave blockages. The double-source configurations with wave blockages in Figs. 9(b) and 9(c) can form a more distant wave focalization than the single point source configuration in Fig. 9(a). The simulation results in Figs. 9(b) and 9(c) clearly confirm that the focusing points i_1, i_2, and $j_{1,2}$ can be removed from the system by applying the half-side wave beam blockages.

The simulation results do not indicate the occurrence of a subwavelength focusing for hybrid focusing points. The half width of the nearest hybrid focusing point ($i_{1,2}$) is observed to be 1.22λ (wavelength of sound wave $\lambda = 2.13$ cm). A future study can be devoted to enhance the resolution of the hybrid focusing points.

6. Conclusion

A point source array placed in front of a sonic crystal flat lens leads to additional focusing points referred to as hybrid focusing points. This study theoretically demonstrated forward and backward hybrid focusing points appearing when a point source array was used as the input of the negative refractive sonic crystal lens. A ray-trace analysis of the multi-source system was conducted for the estimation of hybrid focusing point distances from the sonic crystal lens. A possible use of the forward hybrid focusing point was discussed for the double-source acoustic flat lens design.

The main benefit of the hybrid focusing point is that it allows one to obtain a more distant wave focalization than the pure focusing points. The hybrid focusing points promise new methods for controlling the positions of far-field wave focusing points. In the previous works, the locations of focusing points were adjusted by tuning the distance of the point source to the flat lens (D_1), or adjusting the wave frequency, the lattice or medium parameters.[24,25,34,38–40] This study showed that the distance between point sources (e) can be useful in the control forward hybrid focusing point locations in a wider range without changing any other system parameters. This can be very beneficial to the development of acoustic devices to steer the far-field focusing points. Although the hybrid focusing points can be useful in applications associated with the far-field acoustic energy transmission and harvesting,[41] they lead to an undesired effect in acoustic imaging technologies, since the hybrid focusing points may form false images of the point sources. Therefore, imaging technologies using flat lenses must consider the false image caused by the hybrid focusing points.

References

[1] Zhuang D X, Chen X Y, Li J J, Qiang Z X, Jiang J Z, Chen Z Y, Qiu Y S and Li H 2012 *Chin. Phys. Lett.* **29** 124201

[2] Wang C H, Kuang D F, Chang S J and Lin L 2012 *Chin. Phys. Lett.* **29** 124205

[3] Zhang C X and Xu X S 2012 *Chin. Phys. B* **21** 044213

[4] Tang H X, Zuo Y H, Yu J Z and Wang Q M 2008 *Chin. Phys. B* **17** 228

[5] Zhang H, Guo P, Chang S J and Yuan J H 2008 *Chin. Phys. Lett.* **25** 3898

[6] Shen X X, Yang X L, Cai L Z, Wang Y R, Dong G Y, Meng X F and Xu X F 2008 *Chin. Phys. Lett.* **25** 3972

[7] Zhang X, Chen S W, Liao Q H, Yu T B, Liu N H and Huang Y Z 2011 *Chin. Phys. Lett.* **28** 084201

[8] Wu H, Jiang L Y, Jia W and Li X Y 2012 *Chin. Phys. Lett.* **29** 034203

[9] Hou S L, Xue L M, Li S P, Liu Y J and Xu Y Z 2012 *Acta Phys. Sin.* **61** 134206 (in Chinese)

[10] Sun W Q, Liu Y M, Wang D L, Han L H, Guo X and Yu Z Y 2013 *Chin. Phys. B* **22** 014201

[11] Feng S, Ren C, Wang W Z and Wang Y Q 2012 *Chin. Phys. B* **21** 114212

[12] Zhu Q Y, Fu Y Q, Hu D Q and Zhang Z M 2012 *Chin. Phys. B* **21** 064220

[13] Jiang H, Zhang M L, Wang Y R, Hu Y P, Lan D and Wei B C 2009 *Chin. Phys. Lett.* **26** 106202

[14] Ni Q and Cheng J C 2005 *Chin. Phys. Lett.* **22** 2305

[15] Gao X W, Chen S B, Chen J B, Zheng Q H and Yang H 2012 *Chin. Phys. B* **21** 064301

[16] Kong X Y, Yue L L, Chen Y and Liu Y K 2012 *Chin. Phys. B* **21** 096101

[17] Zhong L H, Wu F G and Zhong H L 2010 *Chin. Phys. B* **19** 020301

[18] Zhu X F, Liu S C, Xu T, Wang T H and Cheng J C 2010 *Chin. Phys. B* **19** 044301

[19] Cai C, Zhu X F, Chen Q, Yuan Y, Liang B and Cheng J C 2011 *Chin. Phys. B* **20** 116301

[20] Li Y, Hou Z L, Fu X J and Badreddine M A 2010 *Chin. Phys. Lett.* **27** 074303

[21] Zhang S, Hua J and Cheng J C 2003 *Chin. Phys. Lett.* **20** 1303

[22] Jiang H, Wang Y R, Zhang M L, Hu Y P, Lan D, Wu Q L and Lu H T 2010 *Chin. Phys. B* **19** 026202

[23] Qin B, Chen J J and Cheng J C 2005 *Chin. Phys.* **14** 2522

[24] Qiu C, Zhang X and Liu Z 2005 *Phys. Rev. B* **71** 054302

[25] Alagoz S and Alagoz B B 2009 *Appl. Acoust.* **70** 1400

[26] Alagoz S 2012 *Chin. J. Phys.* **50** 703

[27] Yang S, Page J H, Liu Z, Cowan M L, Chan C T and Sheng P 2004 *Phys. Rev. Lett.* **93** 024301

[28] Alagoz S 2012 *Chin. Phys. B* **21** 126202

[29] Feng Z F, Wang X G, Li Z Y and Zhang D Z 2008 *Chin. Phys. B* **17** 1101

[30] He Z, Li X, Mei J and Liu Z 2009 *J. Appl. Phys.* **106** 026105

[31] Sukhovich A, Merheb B, Muralidharan K, Vasseur J O, Pennec Y, Deymier P A and Page J H 2009 *Phys. Rev. Lett.* **102** 154301

[32] Zhao H G, Wen J H, Liu Y Z, Yu D L, Wang G and Wen X S 2008 *Chin. Phys. B* **17** 1305

[33] Cai C, Zhu X F, Chen Q, Yuan Y, Liang B and Cheng J C 2011 *Chin. Phys. B* **20** 116301

[34] Sanchez-Morcillo V J, Staliunas K, Espinosa V, Pérez-Arjona I, Redondo J and Soliveres E 2009 *Phys. Rev. B* **80** 134303

[35] Economou E N and Sigalas M M 1993 *Phys. Rev. B* **48** 13434

[36] Miyashita T 2005 *Meas. Sci. Technol.* **16** 47

[37] Wang W C, Wu L Y, Chen L W and Liu C M 2010 *Smart Mater. Struct.* **19** 045016

[38] Feng Z F 2010 *Chin. Phys. B* **19** 067201

[39] Wu L Y, Yang W P and Chen L W 2008 *Phys. Lett. A* **372** 2701

[40] Deng K, Ding Y, He Z, Zhao H, Shi J and Liu Z 2009 *J. Phys. D: Appl. Phys.* **42** 185505

[41] Wang W C, Wu L Y, Chen L W and Liu C M 2010 *Smart Mater. Struct.* **19** 045016